Solubilization of a Homopolymer in a Block Copolymer

Kyung-Jin Jeon and Ryong-Joon Roe*

Department of Materials Science and Engineering, University of Cincinnati, Cincinnati, Ohio 45221

Received November 10, 1993; Revised Manuscript Received February 11, 1994•

ABSTRACT: Blends containing styrene–butadiene diblock copolymer (50 wt % styrene content) and polystyrene of various molecular weights are studied by light scattering, transmission electron microscopy, and small-angle X-ray scattering. The solubility of polystyrene in the styrene domain of the block copolymer is governed by the ratio of the homopolymer molecular weight to the block molecular weight. A finite solubility limit exists when this ratio exceeds ~1. The lamellar repeat period increases linearly as more polystyrene is added, but the butadiene layer thickness remains constant, signifying that the average interfacial area occupied by a copolymer junction point does not change with added polystyrene. This contrasts to the case found by others that the average area per junction point increases when the added homopolymer is smaller than the block size. Small-angle X-ray scattering patterns obtained from samples having lamellar morphology are described by an idealized model in which layers of styrene and butadiene of randomly varying thicknesses with a diffuse interface between them are stacked parallel.

Introduction

Diblock copolymers show a rich variety of morphologies depending on the relative lengths of the two blocks and the temperature (or the strength of interaction between the blocks). The material exists as a disordered phase at high temperatures but on cooling undergoes a microphase separation into an ordered phase, which exhibits a spherical, ordered bicontinuous double diamond (OBDD), cylindrical, or lamellar structure. When a homopolymer is mixed with a diblock copolymer, the two may mix into a single homogeneous phase (with or without a microdomain order) or separate into two macrophases, depending on the temperature and the relative amounts of the two components. The two types of phase separations, i.e., microphase and macrophase separation, interact with each other, producing added possibilities for phase transitions. The phase diagrams[1,2] that result are consequently rich in fascinating complexities. Adding homopolymers to block copolymers thus opens a new avenue for producing materials with interesting morphologies and novel properties. Many of the features observed in these phase diagrams[2] are as yet only poorly understood. No systematic experimental studies have so far been performed to show how the phase diagram might change when some of the molecular parameters, for example, the lengths of the homopolymer or the copolymer blocks, are altered. In addition, several of the phases identified in the phase diagrams[2] were only poorly defined and need to be characterized in more detail experimentally. Although some theoretical studies[3–6] have been made to predict phase diagrams under more general conditions, their validity has not yet been thoroughly tested against experiment. Clearly, there is a need for more systematic experimental studies.

In this work we take two styrene–butadiene diblock copolymers (of about 50/50 composition) of two different sizes to which polystyrenes of various sizes are added. We are interested in finding out, among other things, the solubility limit of the homopolymer and its dependence on the size of the polymers involved, the change in the structure of the microdomains as the homopolymer concentration is increased within the solubility limit, and the way new morphologies evolve as the solubility limit is eventually exceeded. We are interested in studying these events in the strong segregation limit, that is, at temperatures far below the microphase separation temperature. For this purpose we combine the techniques of small-angle X-ray scattering, transmission electron microscopy, and light scattering, the first two to study the microphase morphology and the last to determine the turbidity of the sample as the indicator of an onset of macrophase separation.

• Abstract published in *Advance ACS Abstracts*, March 15, 1994.

Table 1. Characteristics of the Polymers Used

	sample label	M_n(GPC)	M_w/M_n	styrene content (wt%)	note
diblock copolymer	SB25	25 000	1.04	52.0	*a*
	SB48	47 900	1.04	51.1	*b*
polystyrene	S15	14 600	1.03	100	*c*
	S18	18 100	1.06	100	*d*
	S25	24 500	1.07	100	*c*
	S30	30 000	1.03	100	*e*
	S45	45 500	1.05	100	*e*

[a] Synthesized by Dr. H. L. Hsieh of Phillips Petroleum Co. [b] Synthesized by Dr. L. H. Tung of Dow Chemical Co. [c] Synthesized in our laboratory. [d] Purchased from Scientific Polymer Products, Inc. [e] Purchased from Pressure Chemical Co.

Experimental Procedures

The characterization data of the polymers used are listed in Table 1. The polymers, from various sources, were all prepared by anionic polymerization. Note that the two styrene–butadiene diblock copolymers used are nearly symmetrical in their comonomer contents, and the larger of two, SB48, is almost exactly twice the other, SB25, in overall size. In the following, a mixture sample is designated by the labels of the two polymers involved, followed by their weight percentages in parentheses, as in "SB25/S15 (91/09)". The blend composition can also be specified by the overall volume fraction ϕ_s of the styrene monomer in the blend (including the contributions from both the homopolymer and the styrene block). To convert from weight to volume, the densities 1.059 g/cm^3 for polystyrene and 0.896 g/cm^3 for polybutadiene at room temperature were used. The composition in terms of the styrene volume fraction is useful when comparing with results obtained with block copolymers having a symmetry different from ours. A third way of designating the blend composition is to consider only the constituents in the styrene microdomains (assuming that all of the homopolymer is actually in the styrene microdomains and nowhere else) and to specify the fraction p of the styrene monomeric units in them that belong to the homopolymer. This is useful in describing the solubility of the homopolymer within the styrene domains.

0024-9297/94/2227-2439$04.50/0

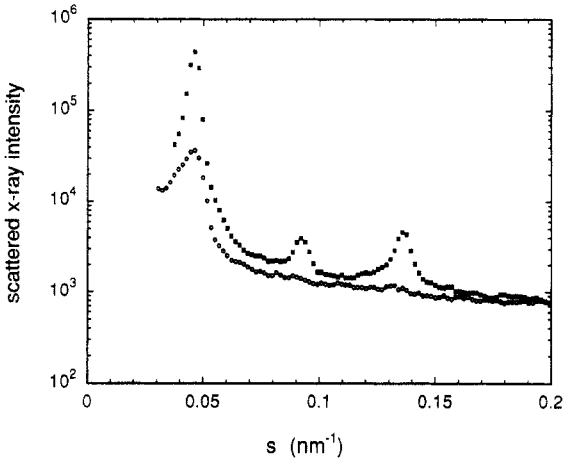

Figure 1. Small-angle X-ray intensity curves obtained with an oriented film of SB25/S15 (91/09) plotted against s (=2 sin θ/λ). The filled and open symbols are the data taken with the film parallel and perpendicular, respectively, to the film surfaces.

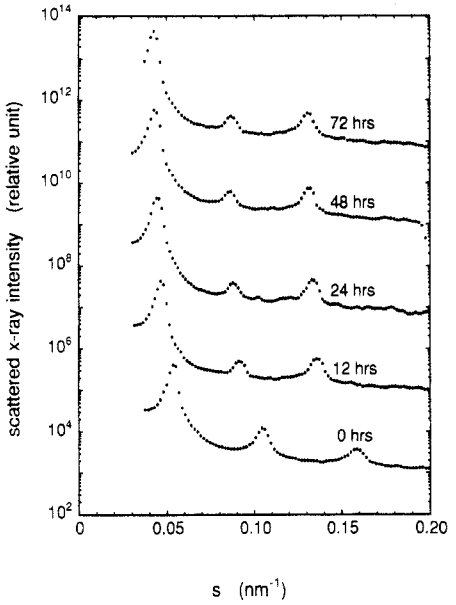

Figure 2. Small-angle X-ray intensity curves obtained with SB25/S15 (91/90) after annealing at 130 °C for various lengths of time as indicated. Curves are shifted vertically for legibility.

Small-angle X-ray scattering measurements were performed with a Kratky camera fitted with a Braun linear position-sensitive detector. Ni-filtered Cu Kα radiation from a Philips XRG 3100 generator operating at 45 kV and 35 mA was used. Corrections for detector sensitivity and nonlinearity and for background scattering were applied, but not for slit smearing. Oriented specimens for small-angle X-ray measurements were prepared as follows. A mixture of diblock copolymer with homopolymer was dissolved in benzene to make a 4% solution. The solution was cast on a glass plate, and the solvent was evaporated slowly at room temperature for 3 days. Many sheets of dry films thus prepared, each of ~0.1-mm thickness, were stacked together in parallel to form a sample of ~3-mm total thickness, which was kept under a vacuum at room temperature for several more days until constant weight and then annealed for 3 days at 130 °C.

The degree of lamellar alignment achieved in such a sample can be gauged from Figure 1, in which the small-angle X-ray scattering intensity curve obtained with the sample mounted to have the film surface parallel with the X-ray beam is compared against the one obtained with the surface perpendicular to the X-ray beam. The effect of annealing on the lamellar structure can be seen from Figure 2, where the X-ray scattering intensities with SB25/S15 (91/09) obtained after varying lengths of annealing at 130 °C are given against s (=2 sin θ/λ). The d spacings evaluated from the scattering curves are 19.0, 21.4, 21.9, 22.5, 22.6, and 22.6 nm after 0, 12, 24, 48, 72, and 168 h of annealing, respectively. This shows that in this sample 3 days of annealing at 130 °C is sufficient to erase the memory imparted during the solvent casting and to cause the sample to approach an equilibrium structure.

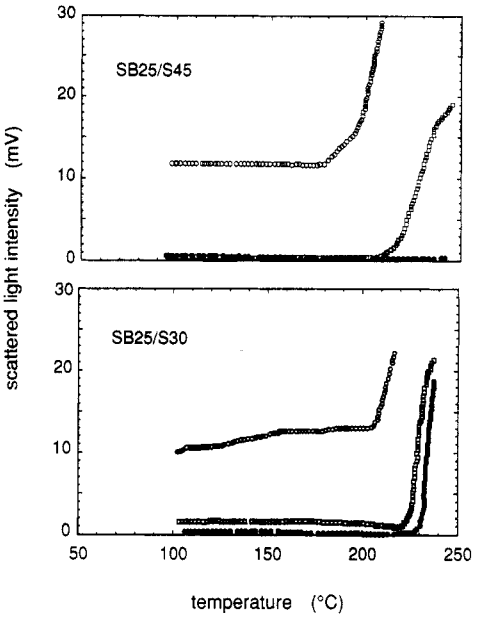

Figure 3. Intensities (output of the photodiode in millivolts) of light scattered from (a) SB25/S45 (filled circles for 985/015, open squares for 97/03, open circles for 96/04) and (b) SB25/S30 (filled circles for 92/08, open squares for 91/09, open circles for 88/12). Note that for each sample the intensity increases rapidly beyond a certain temperature and that the low-temperature intensity depends on the composition of the blend.

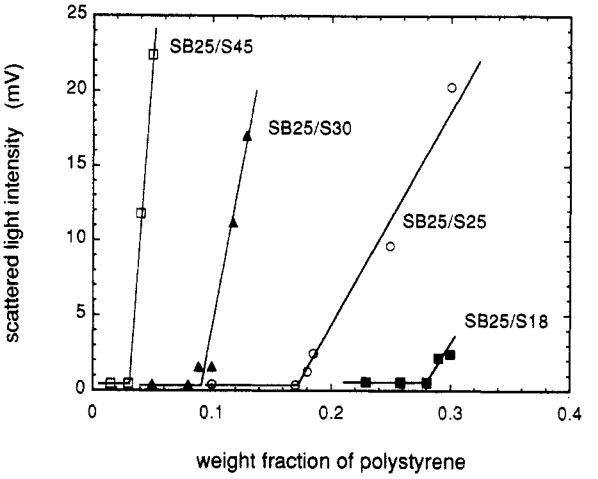

Figure 4. Scattered light intensities measured at 130 °C plotted against the composition of the blends: open squares for SB25/S45, filled triangles for SB25/S30, open circles for SB25/S25, and filled squares for SB25/S18. The points at which the scattered intensity starts to increase rapidly are taken as marking the limit of solubility of added polystyrene in the styrene domains of the block copolymer.

Samples for electron microscopy were exposed to OsO_4 vapor for 23 h, embedded in epoxy resin, and microtomed with a diamond knife at ~−70 °C. The sections, 40–60 nm in thickness, were stained with OsO_4 again for 24 h and examined under a Philips CM20 transmission electron microscope at 100–150 kV. Light scattering measurements were performed with a low-power He–Ne laser beam impinging on the sample and a photodiode detecting the light scattered at either 90 or 60°. Unoriented samples for electron microscopy and light scattering were prepared either by melt blending (without solvent) under vacuum at elevated temperature in the case of lower molecular weight materials or by casting from toluene solution in the case of higher molecular weight materials.

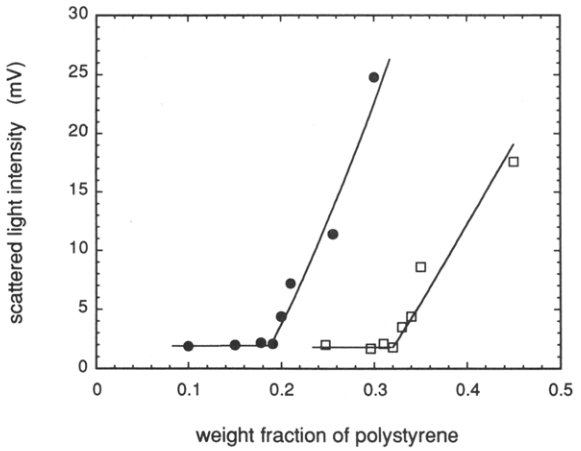

Figure 5. Similar to Figure 4, but the filled circles are for SB48/S45 and the open squares for SB48/S30.

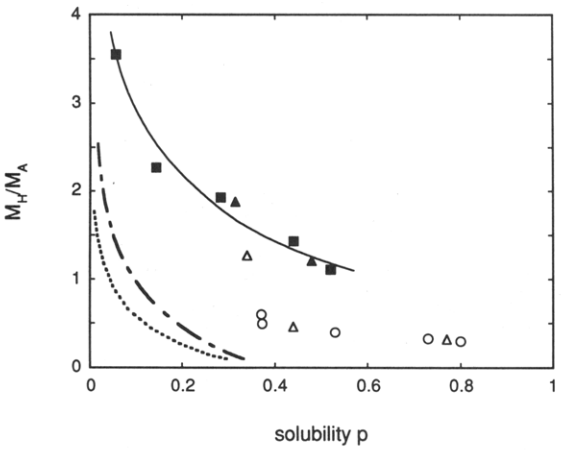

Figure 6. Solubility limits of polystyrene in styrene–butadiene block copolymer obtained by various workers plotted against the ratio M_H/M_A, where M_H and M_A are the molecular weights of polystyrene and styrene block in the copolymer, respectively. The solubility is expressed as the fraction p that belongs to the homopolymer among the styrene repeat units in the styrene microdomains. The filled squares are for blends containing SB25, and the filled triangles are for blends containing SB48, both of which exhibit lamellar morphology. The solid line is a guide to the eye drawn through these two sets of data. The open triangles show the data[2] obtained with an asymmetric diblock copolymer exhibiting spherical microdomains of styrene, and the open squares show those[7] obtained with a triblock copolymer exhibiting a cylindrical morphology. The dotted line and the dot–dash line give the solubility limits calculated by the theories due to Meier[21] and to Tucker and Paul,[22] respectively.

Results

1. Light Scattering. The intensity of scattered light was recorded with each sample as the temperature was raised slowly from room temperature to ~240 °C. Some examples of the recorded data are shown in Figure 3. The general pattern observed is that initially the scattered intensity remains fairly steady for an extended temperature range, until the intensity starts to rise rapidly beyond a certain temperature. This temperature depends on the composition and the sizes of the polymers involved in the blend. This sudden increase in turbidity undoubtedly indicates an onset of macrophase separation of some kind, but its significance is discussed later in the Discussion. At present, we mainly focus on the state of the blends at 130 °C, the temperature at which samples for electron microscopy and small-angle X-ray measurement were annealed. The scattered light intensities measured at 130 °C plotted against composition of the blends are shown in Figure 4 for samples that contain block copolymer SB25 and in Figure 5 for samples that contain SB48. The point at which the scattered intensity starts to rise sharply with increasing amount of added polystyrene is taken as the solubility limit. We note that, with some blends, especially with those containing SB48, some turbidity is noticeable even before the solubility limit is reached, but this does not prevent us from recognizing a sudden onset of increased turbidity with good accuracy. With blends SB25/S15 and SB48/S25, both containing a polystyrene of roughly the same size as the styrene block in the copolymer, no sign of reaching and exceeding a solubility limit could be found at any composition.

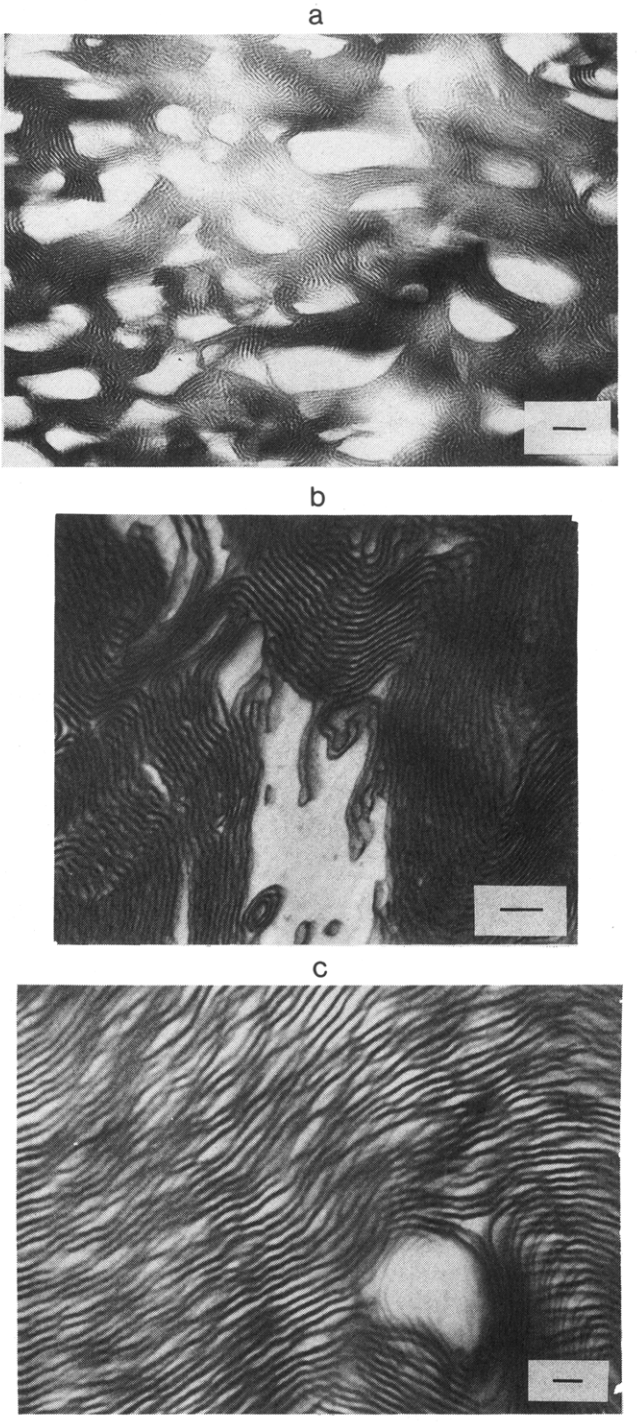

Figure 7. Morphologies of blends containing polystyrene beyond the solubility limits: (a, top) for SB25/S45 (85/15); (b, middle) for SB25/S30 (70/30); (c, bottom) for SB48/S45 (68/32). The scale bars represent 100 nm.

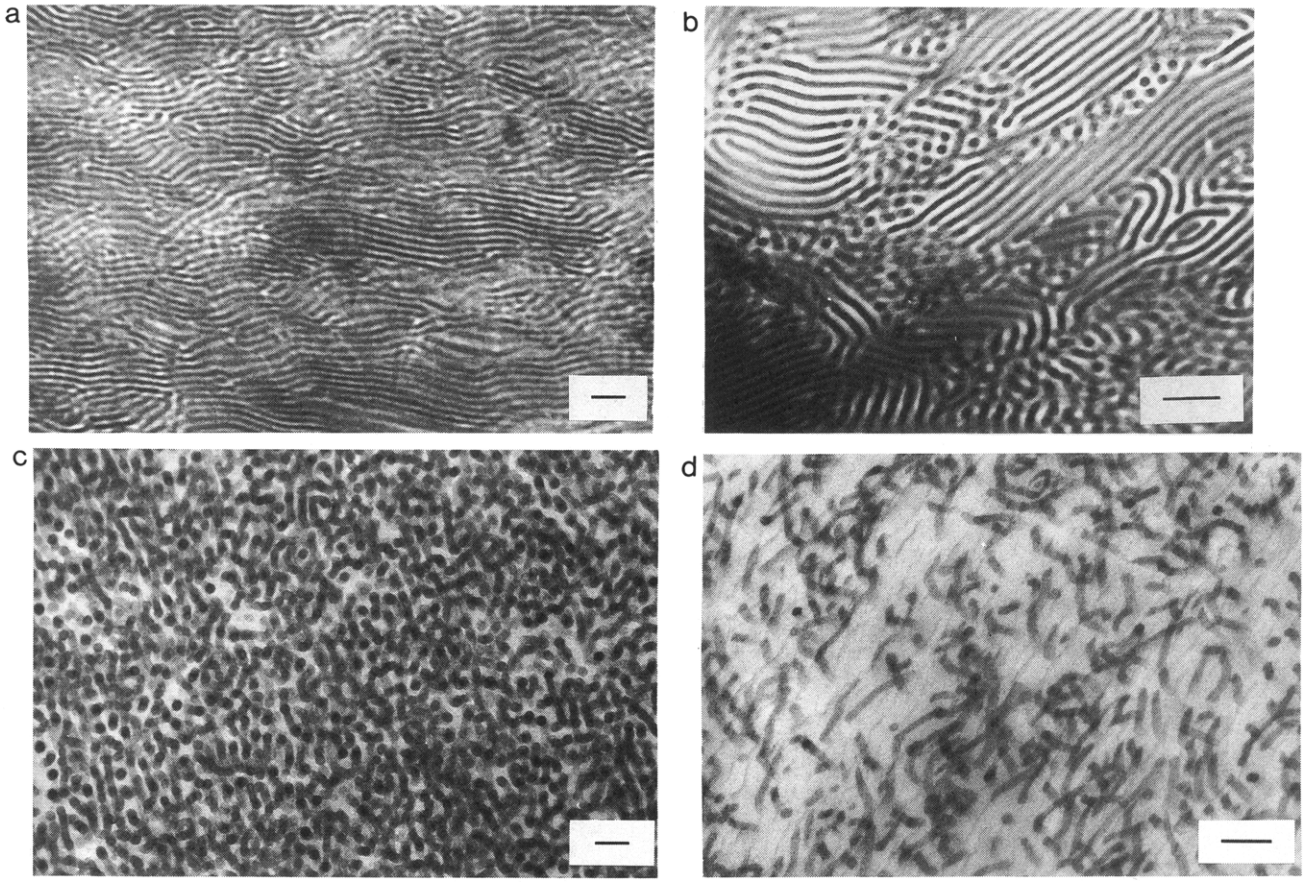

Figure 8. Blend SB48/S25, having no limit to solubility of polystyrene, shows varied morphologies as the polystyrene concentration is increased: (a, top left) for 82/18; (b, top right) for 65/35; (c, bottom left) for 35/65; (d, bottom right) for 15/85. The scale bars represent 100 nm.

The solubility limits determined from Figures 4 and 5 are plotted in Figure 6 against the ratio M_H/M_A, where M_H and M_A are the molecular weights of the polystyrene and the styrene block in the copolymer, respectively. (The solubility p is here expressed, as remarked before, as the fraction of styrene monomer in the styrene microdomains that belong to homopolymer.) The data obtained with SB25 and SB48 merge into a single curve, confirming that it is relative, and not the absolute, sizes of the homopolymer and the block copolymer that govern the solubility behavior. Figure 6 also gives solubility data of polystyrene in styrene–butadiene block copolymer taken from the literature. The open triangles denote those[2] obtained with blends containing a diblock copolymer in which the styrene and butadiene block molecular weights are 7300 and 19 700, respectively. The open circles are those[7] obtained with blends containing a triblock copolymer with the following block molecular weights: styrene, 10 430; butadiene, 53 600; styrene 10 430. One can see that the solubilities of polystyrene in these nonsymmetrical block copolymers are very much smaller than the present results involving symmetrical diblock copolymers. This probably reflects the difference in the morphology, since our samples are lamellar whereas the nonsymmetrical copolymers give spherical or cylindrical morphology, which not surprisingly has a greater difficulty in accommodating guest homopolymer molecules.

2. Electron Microscopy. In the absence of added homopolymer the block copolymers, SB25 and SB48, used in this work present a well-developed lamellar structure. As the amount of added polystyrene is increased, the regular lamellar order is increasingly disturbed. To describe it, we have to distinguish the behaviors of the blends that eventually reach a solubility limit (SB25/S45, SB25/S30, SB25/S25, SB25/S18, SB48/S45, and SB48/S30) and those without such a limit (SB25/S15, SB48/S25, and SB48/S15).

With those blends exhibiting a solubility limit, the interesting point is to see the development of polystyrene-rich macrophases dispersed within the matrix of block copolymer phase. Three examples of such blends, obtained with SB25/S45 (85/15), SB25/S30 (70/30), and SB48/S45 (68/32), are given in Figure 7. With all three examples, the lamellar structure in the matrix phase is retained but is disturbed to varying degrees. Example c shows the styrene lamellar thickness that has expanded unevenly along its lamellar planes. In the case of example b, the polystyrene macrophase contains an open network of faintly-dark irregular threads suggesting a possible presence of planar micelles in it, a feature which is clearly seen in the original micrograph but may not be readily recognizable in the reproduction given here.

With samples without a solubility limit, the range of blend compositions that can be examined is wider, and the morphological features also show a much wider variation. Figure 8 shows a series of four micrographs obtained with SB48/S25 containing increasing amounts of polystyrene: (82/18), (65/35), (35/65), and (15/85). At 18% homopolymer (a), the lamellar structure is still well maintained, but at 35% (b), a new mophological feature becomes mixed with lamellae. In a previous publication,[8] a detailed analysis was presented to show that at 40% polystyrene the blend displays a well-developed morphology termed a catenoid–lamellar structure, in which the butadiene layer is periodically punctured with catenoid-shape intrusion of styrene-rich channels. Figure 8 suggests that at 35%, the blend consists of a mixture of lamellar structure with such a catenoid–lamellar structure. At 65%

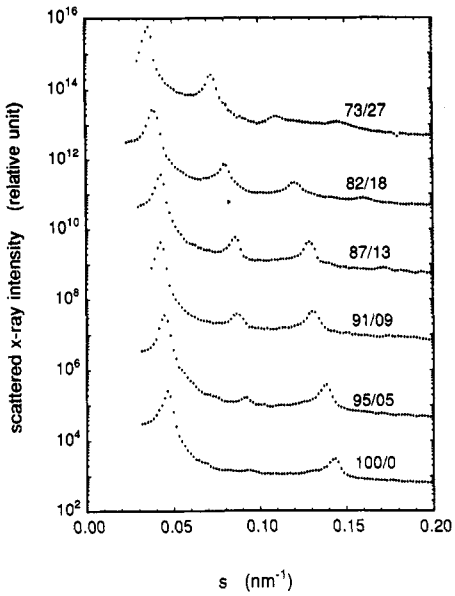

Figure 9. X-ray intensities scattered from blend SB25/S15 containing various amounts of polystyrene as indicated. Curves are shifted vertically for legibility.

in (c) the structure degenerates into an irregular network of butadiene "struts",[9] which on further dilution with polystyrene, at 85%, turn into what looks like cylindrical micelles. With blends other than SB48/S25, the catenoid-lamellar structures has not yet been observed.

3. Small-Angle X-ray Scattering. Figure 9 shows the X-ray scattering intensities obtained with SB25/S15 samples containing various concentrations of polystyrene. The higher order peaks for each sample occur at s values which are exact multiples of the first-order peak, indicating that the morphology is lamellar. As the polystyrene content is increased, the peak positions shift toward smaller angles, showing that the lamellar periodicity increases. At the same time, the relative heights of the peaks change. With neat block copolymer, the even-order peaks are almost completely absent, reflecting the symmetry of the block copolymer. With increasing addition of polystyrene, the styrene layer becomes thicker than the butadiene layer, and this causes the relative heights of even vs odd peaks to change. With other blend samples, the trend with increasing polystyrene content is similar, except that with samples containing SB48 peaks up to the sixth order are visible. The lamellar period d evaluated from the peak positions is plotted in Figure 10 against the composition of the blend. The estimated error bars are equal to or smaller than the size of the symbols in the figure. In the case of copolymer SB25, the lamellar period increase is seen to depend only on the amount, and not on the size, of the added polystyrene. In the case of SB48, the data suggest the possibility that the lamellar period increase may depend on the size of the polystyrene as well. Figure 10 includes data for SB48/S45 and SB25/S25 only up to the solubility limits. When data beyond the solubility limits are included, as in Figure 11, the lamellar period is seen to stop growing with further increases in the added polystyrene, and the point at which this occurs agrees well with the solubility limit determined from the turbidity measurements.

Because the relative volumes of the styrene and butadiene microdomains are known (on the assumption that intermixing of styrene and butadiene units is totally excluded), one can divide the measured lamellar period d into the thicknesses d_S and d_B of the styrene and butadiene layers. Figures 12 and 13 plot the variation of these

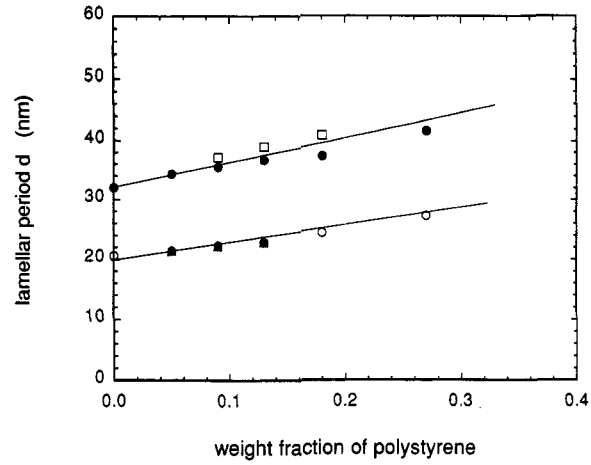

Figure 10. Lamellar periods evaluated from peaks in the X-ray intensity curves plotted against the composition of the blends: filled circles for SB48/S25, open squares for SB48/S45, open circles for SB25/S15, and filled triangles for SB25/S25.

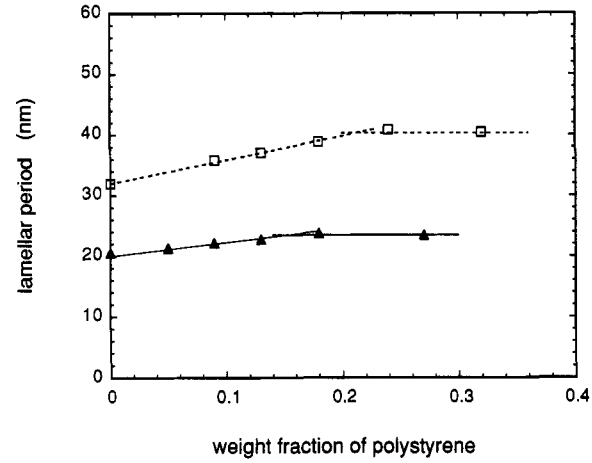

Figure 11. The lamellar period stops growing with increasing concentration of added polystyrene when the solubility limits of the latter are exceeded in the case of SB48/S45 (open squares) and SB25/S25 (filled triangles).

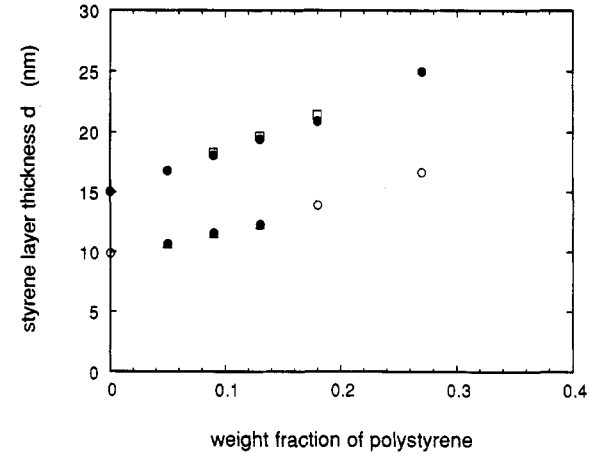

Figure 12. Thickness of styrene microdomain layer against the composition of the blend: filled circles for SB48/S25, open squares for SB48/S45, open circles for SB25/S15, and filled triangles for SB25/S25.

thicknesses with blend composition. Figure 13 shows that the butadiene layer thickness remains approximately constant. This means that, even with a growing addition of polystyrene, the interfacial area per block copolymer junction is unaltered, or, in other words, the structure of the butadiene layer suffers neither expansion nor compression in any direction.

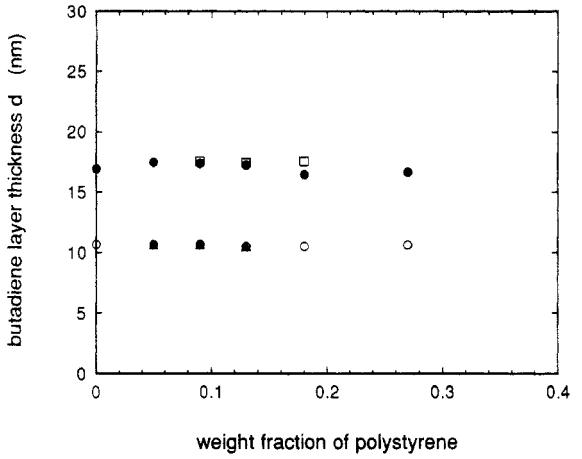

Figure 13. Thickness of butadiene microdomain layer against the composition of the blend: filled circles for SB48/S25, open squares for SB48/S45, open circles for SB25/S15, and filled triangles for SB25/S25.

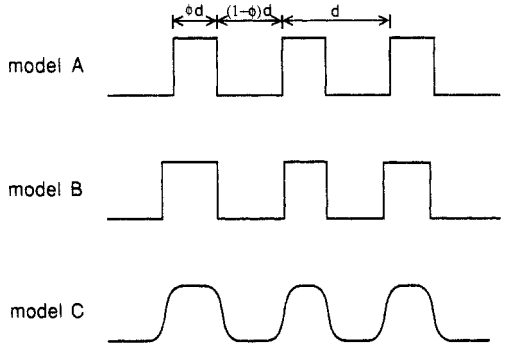

Figure 14. Electron density variation in idealized one-dimensional models of stacks of lamellae.

Analysis of SAXS Curves

To interpret the X-ray scattering patterns such as those shown in Figure 9, we will construct simple models of lamellar structure and compare the calculated curves with observed ones. Similar analyses have previously been presented by other workers.[10,11] The change in the relative heights of even- vs odd-order peaks with the composition can be seen most clearly by considering the simplest structure shown in Figure 14. Here model A depicts a perfectly regular stack of alternating layers of styrene and butadiene, with the layer thicknesses exactly equal to $d\phi$ and $d(1-\phi)$, respectively, and the interface between them infinitely sharp. The electron density $\rho_A(z)$ in the direction z perpendicular to the lamellar plane can then be expressed as

$$\rho_A(z) = \rho_1 + \Delta\rho\Pi\left(\frac{z}{\phi d}\right) * \Delta\left(\frac{z}{d}\right) \tag{1}$$

where $\Pi(z)$ is a step function defined by

$$\begin{aligned} \Pi(z) &= 0 \quad \text{for } |z| > {}^1/_2 \\ &= 1 \quad \text{for } |z| < {}^1/_2 \end{aligned} \tag{2}$$

$\Delta(z)$ is an infinite series of δ functions

$$\Delta(z) = \sum_{n=-\infty}^{\infty} \delta(z-n) \tag{3}$$

and "*" denotes a convolution product. By taking the square of the Fourier transform of (1), we obtain the scattered X-ray intensity to be proportional to

$$I_A(s) = \Delta(ds)\frac{d}{2\pi^2 s^2}[1 - \cos(2\pi s d\phi)] \tag{4}$$

The intensity function consists of a series of δ functions located at $s = n/d$, where n is an integer. The intensity of the nth-order peak is therefore proportional to $[1 - \cos(2\pi n\phi)]/n^2$. This shows that the relative heights of the successive peaks are governed only by ϕ, which depends on the relative thickness of the two layers. When the two layers are of equal thickness, ϕ is equal to ${}^1/_2$, and this leads $1 - \cos(2\pi n\phi)$ to vanish at even n.

In reality, the thicknesses of the styrene or butadiene layers in the stack are not perfectly uniform, and this leads to smearing of the δ functions in (4) into broader peaks. Model B in Figure 14 depicts the case where the thicknesses fluctuate around their mean ϕd and $(1-\phi)d$ but the lamellae are still perfectly parallel to each other and the interface is infinitely sharp. An exact solution for such a model was derived by Hosemann and Bagchi.[12] The intensity is now proportional to

$$I_B(s) = \frac{1}{(2\pi s)^2}\frac{|1-F_1|^2(1-|F_2|^2) + |1-F_2|^2(1-|F_1|^2)}{|1-F_1F_2|^2} \tag{5}$$

where F_1 and F_2 are the Fourier transforms of the functions $G_1(z)$ and $G_2(z)$ giving the distributions of the thicknesses of layers 1 and 2, respectively. If we assume the distributions to be Gaussian, with the mean thicknesses equal to $d\phi$ and $d(1-\phi)$ and the standard deviations equal to σ_1 and σ_2, respectively, then F_1 and F_2 are given by

$$F_1(s) = \exp(-2\pi^2 s^2 \sigma_1^2)\exp[-i(2\pi s)\phi d] \tag{6}$$

and

$$F_2(s) = \exp(-2\pi^2 s^2 \sigma_2^2)\exp[-i(2\pi s)(1-\phi)d] \tag{7}$$

The relative heights of even vs odd peaks given by (5) still depend on the fraction ϕ of the volume belonging to layer 1, but this fact is less transparent here than in eq 4. Equation 5 becomes equivalent to eq 4 in the limit of $\sigma_1 \to 0$ and $\sigma_2 \to 0$.

In model C we allow the interface to be diffuse. The electron density distribution $\rho_C(z)$ can be given by the convolution product of $\rho_B(z)$ with a "smearing function" $h(z,t)$

$$h(z,t) = \frac{1}{t}\operatorname{sech}^2\left(\frac{2z}{t}\right) \tag{8}$$

where t is the effective thickness of the interface. The scattered X-ray intensity is then given[13] by

$$I_C(s) = I_B(s)\,H^2(s) \tag{9}$$

where $H(s)$ is the Fourier transform of $h(z,t)$, or[14]

$$H(s) = \frac{\pi^2 ts}{2}\operatorname{csch}\left(\frac{\pi^2 ts}{2}\right) \tag{10}$$

The effect of multiplying with $H^2(s)$ in (9) is to make the intensity $I_C(s)$ fall more rapidly than $\sim s^{-2}$ for large s.

Before we can test how well eq 9 fits the observed intensity curves, there are two additional factors that have to be taken into account. First, the observed intensity contains a contribution from scattering due to thermal density fluctuations, which increases slowly with s and eventually continues to the "amorphous halo" at large s. Such a "background scattering" was estimated by fitting[15]

$$I_b = a + bs^4 \quad (11)$$

with adjustable constants a and b to the tail section ($s > 0.2$ nm^{-1}) of the observed intensity curves. Second, the observed intensity may be smeared due to the incident beam collimation error. Our samples were prepared by stacking thin cast films, and if the layers are in fact oriented perfectly parallel, there is no need to apply a slit length desmearing even when a slit collimation has been used. However, a smearing due to a finite slit width would still be present. The primary beam profile measured in our Kratky camera is an almost perfect equilateral triangle with the base equal to 0.0092 nm^{-1} (in s). The observed intensity curve may then be "desmeared" by a deconvultion process before comparing with the theoretical curve given by eq 9 or, alternatively, the theoretical curve may be first smeared by convoluting with the beam profile before comparing with the smeared experimental curve. We chose to take the second approach, which is less prone to artifacts due to experimental errors.

In Figure 15 several examples are given in which the experimental curves are compared with calculated curves. The latter were evaluated according to eq 9, to which the effects due to slit width smearing and background scattering according to eq 11 were added. Equation 9 contains five adjustable parameters, the lamellar period d, the volume fraction ϕ of the styrene layer, the standard deviations of the styrene and butadiene layer thicknesses σ_1 and σ_2, and the effective interface thickness t. Each of these parameters affects a different aspect of the calculated curve and can therefore be determined almost independently of others. The lamellar period d is given by the peak positions, and the fraction ϕ of the styrene layer is determined from the relative heights of even- vs odd-order peaks. The peak width, the depth of the valleys between peaks, and the increased broadening of higher order peaks are controlled by the standard deviations σ_1 and σ_2, and the decay of the overall curve in higher s regions, in comparison to an s^{-2} behavior, gives the value of the interface thickness t. Although the variation in the thickness of the styrene layer could conceivably be larger than that of the butadiene layer (see Figure 7), we set $\sigma_1 = \phi\sigma_d$ and $\sigma_2 = (1 - \phi)\sigma_d$ in the interest of reducing the number of adjustable parameters. The values of ϕ, σ_d, and t used for the construction of the calculated curves shown in Figure 15 are listed in Table 2.

The agreement is fairly good but is far from being perfect. The best fitting values of ϕ are, in general, larger by about 0.02 than those based on the amount of added polystyrene, for a reason unknown. The interface thickness t turns out to be around 3.0 nm, which is a little larger than the values averaging around 2.0 nm as determined by Porod's law analysis for styrene–isoprene block copolymers.[16] Although the overall shape of the experimental curves is well represented by the calculated ones, the details do not match very well. Adjusting the values of σ_1 and σ_2 independently could have produced a slightly better fit. One of the important reasons for the disagreement may lie in the less-than-perfect parallel ordering of the lamellae in the samples studied. Any disorder in the alignment of layers will make the intensities at larger s fall more rapidly than s^{-2}, leading to an overestimate of the interface thickness t. The misalignment will also make higher order peaks lose strength more rapidly than a truly one-dimensional stack of layers would. This in turn will lead to an overestimation of σ_1 and σ_2 and to the calculated higher order peaks being broader than the observed ones, a trend that is seen in Figure 15.

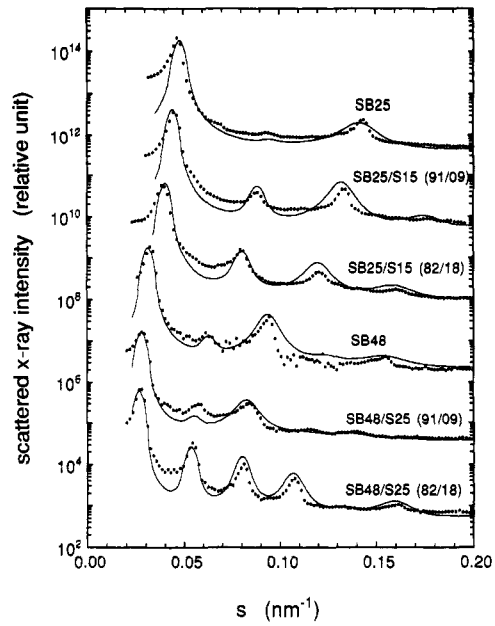

Figure 15. Observed X-ray intensity curves (points) fitted by the curves (solid lines) calculated on the basis of the model discussed in the text.

Table 2. Parameter Values Used To Fit the SAXS Curves

sample	d (nm)	ϕ	σ_d (nm)	t (nm)
SB25	20.9	0.45	1.7	3.0
SB25/S15 (91/09)	22.6	0.54	1.5	2.5
SB25/S15 (82/18)	24.8	0.57	1.8	3.0
SB48	31.8	0.47	2.3	3.0
SB48/S25 (91/09)	35.8	0.53	3.0	3.5
SB48/S25 (82/18)	37.2	0.58	2.0	3.0

Discussion

The change in the microdomain layer thicknesses that occurs with addition of homopolymer A (polystyrene or polyisoprene) in diblock copolymer AB (styrene–butadiene or styrene–isoprene block copolymer) has been studied previously by other workers.[17-19] The main point of interest is whether the added homopolymer forces the lamellae to expand not only in the direction perpendicular to their interfaces but also in the direction parallel to them. An expansion in the parallel direction, if it occurs, means that the homopolymer molecules are penetrating to the junction plane and causing the area per junction point to increase. The answer to this question depends on the molecular weight of the homopolymer in relation to the size of the block in the copolymer. In this study the ratio M_H/M_A is nearly equal to or greater than one. We find that while the styrene layer thickness increases linearly in proportion to the amount of added polystyrene, the butadiene layer thickness remains constant, or, in other words, the area per copolymer junction point in the lamellar interface stays constant. When the homopolymer was smaller than the corresponding block in the copolymer,[17-19] the area per junction point increased as more homopolymer was added. This tendency to expand the lamellae laterally was more pronounced if the homopolymer size was smaller. We recall the results of theoretical analysis performed by Leibler[20] with respect to the status of block copolymer molecules adsorbed at the interface between two immiscible homopolymer phases. When the homopolymers are relatively small, the adsorbed block copolymers form a "wet brush" in which homopolymers penetrate and swell the monolayer of block copolymers, whereas when the homopolymers are relatively large, the adsorbed block copolymers form a tightly packed monolayer of "dry brush" sandwiched between the two homopolymer phases. Sim-

ilarly, in solubilization of homopolymer in block copolymer lamellae, the segments of copolymers near the junction point remain dry when the homopolymer is large but become wet as the homopolymer is made smaller. The crossover between the dry and wet cases appears to occur around the point $M_H/M_A \sim 1$, when the results from this work and those by others are taken together.

The solubility limits determined from turbidity measurements are given in Figure 6. As remarked in the Results, no finite solubility limits could be detected with blends SB25/S15, SB48/S25, and SB48/S15. This suggests that the crossover from the limited solubility to unlimited solubility occurs again at around $M_H/M_A \sim 1$. This, in a way, reaffirms the commonly-held wisdom that homopolymer is soluble in block copolymer only if the homopolymer is not larger than the corresponding block in the copolymer. This rule, however, apparently applies only when the block copolymer morphology is lamellar. Some years ago Meier[21] considered a simple theoretical model to predict the solubility limit in a lamellar block copolymer. The result calculated from his theory is plotted in Figure 6. A refinement was added to his theory later by Tucker and Paul,[22] and the result calculated from the revised theory is also plotted in Figure 6. Both predicted results substantially underestimate the solubility. This discrepancy probably arises, as pointed out earlier,[2] from the assumption employed in these theories that the added homopolymer A is uniformly distributed in the A layer of the copolymer. Such an assumption may have some partial validity in wet brush cases, but with dry brushes it is clearly untenable. In the theoretical treatment by Kang and Zin[5] this fact was incorporated approximately by assuming a level of homopolymer concentration in the central region of A layer different from that in the interfacial region. Shull and Winey[23] made numerical solutions to the mean field equations describing the conformation of block copolymer molecules and evaluated the composition profile in the blend of homopolymer and block copolymer. The results support the qualitative trend described above concerning the dependence on M_H/M_A of the degree of penetration of homopolymer into the brushes.

This work concerns mainly the effect of molecular sizes on the structure and thermodynamics of blends of homopolymer and block copolymer. The results can be understood best when looked at from the perspective of the overall phase diagram. Figure 16 represents an example of the phase diagram which we believe should apply to many of the blends studied in this work. This is based on the phase diagram previously presented[2] but with a modification to allow for the fact that here the block copolymer forms a lamellar, rather than a spherical, morphology. A diagram containing most of the qualitative features seen here was also obtained by a theoretical treatment by Kang and Zin.[5] Here M_1 and M_2 refer to mesophases containing ordered microdomains, and L_1 and L_2 refer to disordered, liquid-like phases. The order–disorder transition temperatures A of the neat block copolymers SB25 and SB48 are above 240 °C and could not be determined. With addition of homopolymer, the blend system initially remains in phase M_1, retaining a lamellar morphology. As the solubility limit is exceeded with increased addition of homopolymer, the system crosses line E–H or B–E (depending on whether the line E–F–G is higher or lower than the annealing temperature 130 °C). The location of these lines shifts toward the right as the homopolymer is made smaller and eventually goes out of the right bound of the diagram when M_H/M_A drops below about unity. With these systems, mesophase M_1,

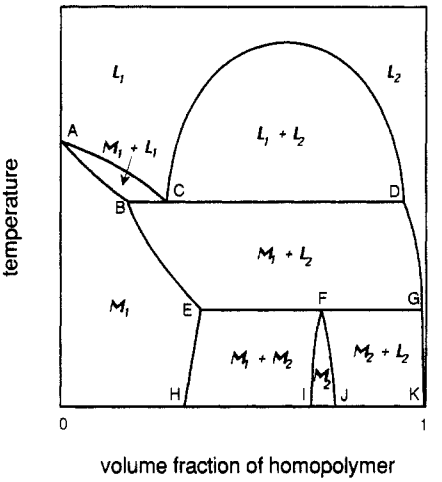

Figure 16. Phase diagram of a blend of a homopolymer with a block copolymer, constructed on the basis of the previously published one,[2] with a minor modification in view of the fact that the block copolymers in this work exhibit lamellar, rather than spherical, morphology. Point A is the order–disorder transition temperature of the block copolymer. For other symbols, see the text and the original publication.[2]

now spanning the whole composition range from 0 to 1, is no longer a single phase but is a succession of mesophases of different morphologies, as Figure 8 shows and as documented by Winey et al.[24] For those systems with solubility limit, M_1 essentially remains a single phase with a lamellar morphology. The polystyrene-rich macrophase that separates out beyond the solubility limit, according to Figure 16, would be a disordered mixture L_2 of polystyrene and block copolymer if the line E–F–G happens to be below the annealing temperature or a mesophase M_2 if it happens to be above the annealing temperature. We believe, on the basis of the following observations, that the latter possibility is actually realized in some of our systems. In Figure 3, showing the turbidity of the blends as a function of temperature, it is seen that the scattered light intensity starts to rise rapidly above a certain temperature, mostly 200 °C or above. This probably signifies crossing line B–E from region M_1 to region $M_1 + L_2$ in Figure 16 in those cases where the low-temperature turbidity is very low [SB25/S45 (97/03), SB25/S30 (92/08)]. When the amount of polystyrene exceeds the solubility limit [SB25/S45 (96/04), SB25/S30 (88/12)], the low-temperature turbidity is already appreciable, and the abrupt, further increase in turbidity corresponds to crossing line E–F from region $M_1 + M_2$ to region $M_1 + L_2$. On the other hand, when the amount of polystyrene is very low [SB25/S45 (98.5/01.5)], raising the temperature will make it cross line A–B from region M_1 to L_1 without encountering any two-phase regions (except for the narrow band $M_1 + L_1$).

Much of the results obtained in this work can be explained, or rationalized, on the basis of the phase diagram given in Figure 16. The data obtained here are, however, not sufficient, by themselves, to allow construction of phase diagrams to any quantitative detail. Collection of much more comprehensive sets of data is required for that purpose. The multitude of features uncovered in this work reinforces the implication of the phrase "fascinating complexity" associated with the phase relationship of blends of homopolymer and block copolymer.

Summary

The structure and phase relationships of blends of styrene–butadiene diblock copolymer and polystyrene

were investigated. Two block copolymers containing ~50 wt % of styrene, one almost exactly twice the size of the other, were employed. The polystyrenes were of varying sizes, some smaller and some larger than the styrene blocks in the copolymers. Light scattering, transmission electron microscopy, and small-angle X-ray scattering were used to examine the characteristics of the blends.

The solubility of polystyrene in the styrene microdomains of copolymer is governed by the ratio M_H/M_A irrespective of the absolute size of the copolymers involved. When this ratio is about equal to or less than one, no limit to the solubility of polystyrene is found. The solubilities obtained in this work, in which the block copolymers form a lamellar structure on their own, are much greater at the same M_H/M_A ratio than those in the block copolymers exhibiting spherical or cylindrical morphologies. With those blend systems showing no solubility limit, a succession of differing morphologies develops as more polystyrene is added, and these include the recently discovered[8] catenoid-lamellar structure.

With increasing polystyrene concentration, the lamellar repeat period expands linearly, but the thickness of the butadiene layer remains constant. This means that the added polystyrene is unable to expand the lamellae laterally and to force the average interfacial area occupied by a copolymer junction point to increase. Other workers have, on the other hand, found that when the added homopolymers were much smaller than the block lengths, the area per junction point increased with increasing homopolymer concentration. The ratio M_H/M_A is thus seen to determine whether the structure attained resembles a "wet brush" or a "dry brush".

Small-angle X-ray scattering patterns obtained from samples having a lamellar morphology can be described well by an idealized model in which layers of styrene and butadiene microdomains of randomly varying thicknesses with a diffuse interface between them are stacked parallel.

Most of the qualitative features obtained in this work can be explained and rationalized on the basis of the phase diagram which incorporates a slight modification to the one previously published.[2] Much more extensive data are, however, required to construct the quantitative details of the phase diagrams, and especially their dependence on the size of the added homopolymer. The multitude of features that are potentially observable with this kind of blend systems make one appreciate the term "fascinating complexity" that is often used to describe the homopolymer–copolymer phase diagram.

Acknowledgment. This work was supported in part by the Petroleum Research Fund, administered by the American Chemical Society. Useful discussions with Drs. M. M. Disko and K. S. Liang are appreciated.

References and Notes

(1) Zin, W. C.; Roe, R. J. *Macromolecules* **1984**, *17*, 183.
(2) Roe, R. J.; Zin, W. C. *Macromolecules* **1984**, *17*, 189.
(3) Hong, K. H.; Noolandi, J. *Macromolecules* **1983**, *16*, 1083.
(4) Whitmore, M. D.; Noolandi, J. *Macromolecules* **1985**, *18*, 2486.
(5) Kang, C. K.; Zin, W. C. *Macromolecules* **1992**, *25*, 3039.
(6) Semenov, A. N. *Macromolecules* **1993**, *26*, 2273.
(7) Han, C. D.; Baek, D. M.; Kim, J.; Kimishima, K.; Hashimoto, T. *Macromolecules* **1992**, *25*, 3052.
(8) Disko, M. M.; Liang, K. S.; Behal, S. K.; Roe, R. J.; Jeon, K. J. *Macromolecules* **1993**, *26*, 2983.
(9) Hashimoto, T.; Koizumi, S.; Hasegawa, H. *Macromolecules* **1992**, *25*, 1433.
(10) Skoulios, A. In *Block and Graft Copolymers*; Burke, J. J., Weiss, V., Eds.; Syracuse University Press: Syracuse, NY, 1973; p 121.
(11) Shibayama, M.; Hashimoto, T. *Macromolecules* **1986**, *19*, 740.
(12) Hosemann, R.; Bagchi, S. N. *Direct Analysis of Diffraction by Matter*; North-Holland: Amsterdam, 1962; p 410.
(13) Ruland, W. *J. Appl. Crystallogr.* **1971**, *4*, 70.
(14) Roe, R. J.; Fishkis, M.; Chang, J. C. *Macromolecules* **1981**, *14*, 1091.
(15) Vonk, C. G. *J. Appl. Crystallogr.* **1973**, *6*, 81.
(16) Hashimoto, T.; Shibayama, M.; Kawai, H. *Macromolecules* **1980**, *13*, 1237.
(17) Ptaszynski, B.; Terrisse, J.; Skoulios, A. *Makromol. Chem.* **1975**, *176*, 3483.
(18) Hashimoto, T.; Tanaka, H.; Hasegawa, H. *Macromolecules* **1990**, *23*, 4378.
(19) Winey, K. I.; Thomas, E. L.; Fetters, L. J. *Macromolecules* **1991**, *24*, 6182.
(20) Leibler, L. *Makromol. Chem., Macromol. Symp.* **1988**, *16*, 1.
(21) Meier, D. J. *Polym. Prepr. (Am. Chem. Soc., Div. Polym. Chem.)* **1977**, *18* (1), 340.
(22) Tucker, P. S.; Paul, D. R. *Macromolecules* **1988**, *21*, 2801.
(23) Shull, K. R.; Winey, K. I. *Macromolecules* **1992**, *25*, 2637.
(24) Winey, K. I.; Thomas, E. L.; Fetters, L. J. *Macromolecules* **1992**, *25*, 2645.